Planar panels and planar supporting beams in architectural structures

CAIGUI JIANG*, Xi'an Jiaotong University, PR China and KAUST, Saudi Arabia
CHENG WANG*, KAUST, Saudi Arabia
XAVIER TELLIER, École des Ponts ParisTech, France
JOHANNES WALLNER, TU Graz, Austria
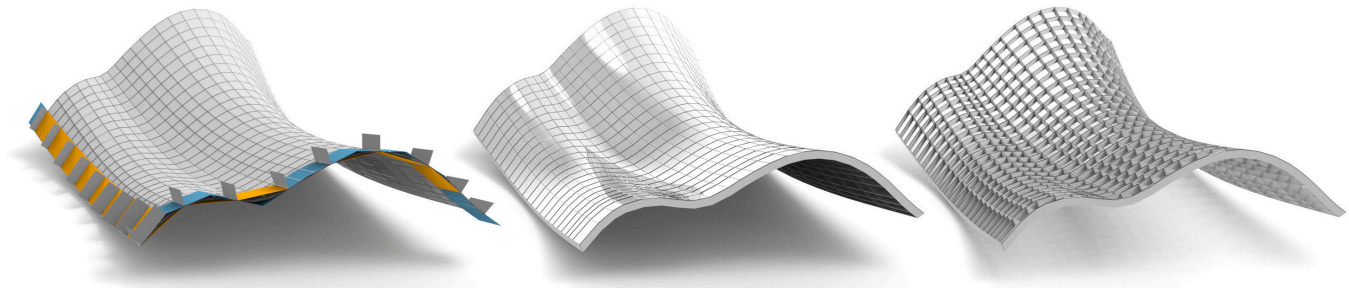HELMUT POTTMANN, KAUST, Saudi Arabia

Fig. 1. This paper deals with the interactive design of meshes with restrictive properties which are nevertheless highly relevant, e.g. for manufacturing. Here we show a control structure for editing a quad mesh with planar faces where both families of mesh polylines have the property that they are entirely contained in a support plane transverse to the mesh. This so-called PP property still leaves sufficiently many degrees of freedom, so we can implement interactive geometric modeling via the colored design handles shown in the left hand image.

In this paper we investigate geometric properties and modeling capabilities of quad meshes with planar faces whose mesh polylines enjoy the additional property of being contained in a single plane. This planarity is a major benefit in architectural design and building construction: if a structural element is contained in a plane, it can be manufactured on the ground without scaffolding and put into place as a whole. Further, the plane it is contained in serves as part of a so-called support structure. We discuss design of meshes under the requirement that one half of mesh polylines are planar ("P-meshes"), and we also investigate the geometry and design of meshes where all polylines enjoy this property ("PP-meshes"). We work in the space of planes and with appropriate transformations of that space. We also incorporate further properties relevant for architectural design, such as near-rectangular panels and repetitive nodes. We provide geometric insights, give explicit constructions, and show an approach to geometric modeling of both P-meshes and PP-meshes, in particular the case of nearly rectangular panels.

CCS Concepts: • **Computing methodologies** → **Shape modeling**; *Optimization algorithms*.

---

*Joint first authors

Authors' addresses: Caigui Jiang, Xi'an Jiaotong University, PR China and KAUST, Saudi Arabia; Cheng Wang, KAUST, Saudi Arabia; Xavier Tellier, École des Ponts ParisTech, France; Johannes Wallner, TU Graz, Austria; Helmut Pottmann, KAUST, Saudi Arabia.

Additional Key Words and Phrases: quad mesh, support structure, planar beams, discrete differential geometry, architectural geometry, Laguerre geometry

1 INTRODUCTION

Many curved structures in architecture are composed of a grid of intersecting beams, each following the edges of a quadrilateral mesh. This article studies situations where many or all of those beams can be manufactured easier because they lie in a plane. There is a long list of actual architectural freeform skins that enjoy this property, and we point only to a few examples. Most are modelled after quad meshes with planar faces. A very practical requirement is that mesh polylines lie in horizontal planes and are thus aligned with floors, see e.g. the *Sail Tower* in Haifa, Israel [Ballas 2003]. Other examples range from small structures like the 2002 Schubert Club "Bandshell" in St. Paul, Minnesota, to medium-sized domes like the roof of the Grand Reading Room, Mansueto Library, Univ. of Chicago, to large buildings like the *Sage Gateshead* concert venue in the UK (Fig. 2). An example where the planes are visually prominent is the Metropol Parasol in Seville, Spain shown by Fig. 3. Structures with planar beams are not restricted to the quad mesh case: a grid without local symmetries supports the glass roof over an interior courtyard at the Dutch maritime museum. And even if a structure is quad based, faces do not have to be planar, as is the case e.g. for the Amtrak train station in Anaheim, California.

Fig. 2. Quadrilateral meshes with planar polylines. The *Sage Gateshead* concert venue, completed in 2004 and designed by Foster+Partners, is based on a quad mesh with planar faces and planar mesh parameter lines.

1.1 Planar Beams in Shell-Like Structures

1.1.1 Planarity of long-range elements. A major reason for planarity of structural elements is easier manufacturing. For timber structures a popular way to fabricate curved beams is via glued laminated timber (*glulam*). Thin layers, usually lumber of standard sizes, are elastically bent and glued together in a curved configuration. It is also possible to make shapes exhibiting torsion that are not contained in a plane, but this process is much more involved. For steel structures, the most common method to produce curved beams is roller bending. This is a manageable task even for varying curvature but is very difficult for non-planar curves. Beams modelled after non-planar curves have to be manufactured in other, more costly, ways.

1.1.2 The P and PP cases of long-range planar beams. In structures where beams cross each other, the actual crossings can be realized in different individual ways. It turns out that this is an important distinction and has strong implications on the global geometry of the structure. Basically two categories have to be distinguished. We call them the P case and the PP case.

• The P case. There are structures where only one sequence of beams continues through crossings uninterrupted, while the transverse beams are short and reach only from one crossing to the next. In such a situation only beams of the first kind present manufacturing challenges so that planarity has to be imposed.

Fig. 3. The *Metropol Parasol* in Seville, Spain, designed by Jürgen Mayer and completed 2011 not features planar mesh parameter lines. The planes carrying parameter are structural elements.

• The PP case. There are also structures where all beams continue through crossings, and then planarity is imposed on all beams. The Schubert Club *bandshell* is an example of this [Schober 2015].

In the Seville *Metropol Parasol* (Fig. 3), only one half of the beams continue through crossings, but planarity is imposed also on the other half. The reason for this is the efficient manufacturing of the load-bearing nodes at crossings [Schmid et al. 2011]. The same is true for the steel structure of the *Sage Gateshead* [Schober 2015].

Planarity of beams has also structural benefits in itself. It ensures that beams can be readily stiffened by auxiliary elements, as has been done for the interior courtyard roof of the Museum of Hamburg History [Ermias et al. 2013]. It also simplifies the fabrication of multi-layer gridshells.

1.1.3 Combining planarity of beams with other properties. Planar beams covering a given surface are, in principle, easily found by intersecting the surface with arbitrary planes. This freedom in design can be used to achieve additional properties.

• Planarity of faces. An important property of this kind is planarity of faces. It allows cladding of the surface with planar panels. Surfaces easily admitting such planar panels are *translation surfaces*, where all beams are parallel translates of two generators. Only special geometric shapes can be achieved in this way, but they have been used several times, e.g. for the above-mentioned Mansueto library [Sobek and Blandini 2010] or the Hippo house in the Berlin zoo [Schober 2015]. Translation surfaces can be efficiently manufactured because of repetitive elements.

• Further properties include an intersection angle of 90° between beams, implying identical nodes and in turn, efficient manufacturing. The Schubert Club "Bandshell" pavillon we mentioned above is an example of this [Schober 2015].

• Another property is funicularity, meaning small bending moments (up to the ideal case of self-supporting surfaces in the sense of Vouga et al. [2012]). An example combining funicularity, planar beams and planar faces is the Dutch Maritime museum [Adriaenssens et al. 2012]. We do not discuss funicularity in this paper.

• Last, but not least, the designer's wishes must be seen as constraints that are imposed on top of geometric properties like planarity of beams and of faces. E.g. for application to architectural facades, it is convenient that upper and lower edges of panels coincide with floor slabs. Imposing this property on many of the occurring planar beams is a strong restriction. We mention this special case to illustrate the fact that a succession of increasing demands reduces the designer's freedom. Planar beams or flat faces alone do not restrict the class of available shapes, only the meshing. However, planar beams plus planar faces plus horizontal floor slabs on top of orthogonal intersection results in a very reduced class of shapes (in this case, the so-called moulding surfaces).

1.2 Contributions and Overview

We study surfaces with long-range planar beams, namely the so-called P and PP cases of one family resp. two families of planar beams covering a design surface. Both are naturally discretized by means of a quad mesh with regular grid combinatorics. Planar beams are discretized as planar mesh polylines (isolated combinatorial singularities occur when individual regular patches are pasted

together). Planar beams are, in principle, easy to achieve since all we have to do is to intersect the design surface with suitable planes. Interesting questions arise if additional properties are required.

Consequently this paper restricts itself to the case of planar faces. The individual contributions of this paper are the following.

— We investigate the P and PP properties for quad meshes with planar faces and completely describe meshes with the PP property (§3.1).
— We study the property of orthogonal intersection of polylines. We argue why this case is best represented by conical meshes and show how to constructively access all possible shapes of such meshes (§§4.1, 4.2 for the PP and P cases, resp.)
— Our methodology is based on the geometry of planes. We therefore give an introduction to Laguerre geometry (§2.1). We also employ torsion-free support structures which were previously proposed in the study of meshes with planar faces. This leads to a new device called the weighted face image (§2.2).
— We discuss different kinds of transformations of meshes which keep the relevant properties we are interested in (§§ 2.3.5, 4.3).
— We discuss different methods of geometric design for meshes. Besides optimization, we make the design space user-friendly by starting from easily accessible and controllable initial shapes and by using transformations for navigation.

The P and PP properties discussed in the present paper restrict the available meshes, even the available shapes, if combined with other properties relevant to architecture. They are thus difficult to achieve by optimization. For this reason our paper extensively discusses explicit constructions of such meshes and how to enable their geometric design.

1.3 Previous Work

The geometric topics touched upon in this paper are more or less classical. Applications of Laguerre geometry to geometric design have been presented by Pottmann and Peternell [1998], and their role in discrete differential geometry is shown by Bobenko and Suris [2007]. Generally, planes instead of points have been used as basic elements of geometric design in several places, e.g. in the dual approach to developable surfaces by Pottmann and Wallner [1999].

A main topic of our paper is representing geometric shapes by planar sections. This has been investigated from the viewpoint of human perception and minimalist representation of shapes [McCrae et al. 2011]. Assembly by interlocking planar pieces is the topic of [Schwartzburg and Pauly 2013].

Our work is about representing geometric shapes by meshes with certain specific properties, namely planar mesh polylines, planar faces, and in addition to that, near-orthogonal intersection of edges. Analogous objects in differential geometry are surfaces with planar parameter lines, with conjugate parameter lines, and in addition to that, with principal parameter lines. The combination of planarity and conjugacy was first studied by [Darboux 1896, vol. IV, ch. IX]. He derived the representation we employ in § 3.1.3.

The more special orthogonal case (surfaces with one or two families of planar principal curvature lines) had been thoroughly studied earlier. Monge [1809] constructed a great variety of such surfaces as sweeping surfaces via the motion of a rotation-minimizing frame.

A special case (rotation-minimizing frame of a planar curve) yields the so-called *moulding surfaces*. For rotation-minimizing frames we refer e.g. to [Bergou et al. 2008; Wang et al. 2008]. Joachimsthal's 1846 result states that the angle between a planar curvature line and its tangent planes is constant. Bonnet [1853], Lemonier [1868] and Serret [1853] used this to determine the equations of such surfaces. Darboux [1896] showed how his representation of planar+conjugate parametrizations specializes to the orthogonal case. We will present a discrete version of his result in § 4.1.

Planar beams and planar faces in freeform architectural skins have recently started to attract interest. Design of special surfaces with one family of principal curvature lines for architectural applications is the topic of Mesnil et al. [2018]. [Tellier 2020; Tellier et al. 2019] employed the classical result by Darboux [1896] and used a discrete model of the Gauss map to obtain circular meshes with planar mesh polylines in both directions. This already represents an approach to the case of meshes with planar beams plus planar faces and near-orthogonal edges. It is the direct motivation for our work, where we broaden the theory and aim at direct and more intuitive methods of design. The main advance of our work compared to [Tellier 2020] is to consider the P case besides the PP case, as well as easier and more comprehensive design methods.

Finally we mention prior work on a different subject (the so-called *multi-nets*) which has an overlap with our work. Bobenko et al. [2020] contains a characterization of meshes with planar faces and planar parameter lines as so-called multi-Q^* nets.

2 GEOMETRIC BASICS

Here we recap the Laguerre geometry of planes (§2.1), describing both planes and spheres as its basic elements, Laguerre transformations of both spheres and planes, and Laguerre transformations of smooth surfaces.

§2.2 introduces the weighted face image, which provides a new viewpoint of torsion-free support structures. It allows us to express the P and PP properties in terms of the shape of dual faces.

§2.3 discusses how further geometric properties (like orthogonality) are expressed in terms of the weighted face image.

2.1 Laguerre Geometry

Geometric arguments in this paper often are concerned with spheres and planes. It is therefore convenient to make use of the well-developed methods of *Laguerre geometry* whose basic entities are spheres, planes, and contact between them. A brief introduction to this topic is given by [Pottmann and Peternell 1998]. For a more comprehensive account see [Cecil 1992].

Both spheres and planes are endowed with an orientation by the choice of a unit normal vector field; oriented contact involves contact in the usual sense plus agreement of unit normal vectors in the point of contact. Formally, two oriented planes are in contact if their unit normal vectors agree (the point of contact is at infinity). A Laguerre transformation is defined as a permutation of the planes, plus a permutation of the spheres, such that oriented contact is preserved. Points are spheres of zero radius. Laguerre transforms in general do not preserve this zero radius property. Points may be mapped to spheres.

2.1.1 Laguerre Transformations of Spheres.
We encode a sphere with center (x, y, z) and signed radius r by the vector

$$X = (x, y, z, r) \in \mathbb{R}^4. \tag{1}$$

We think of a sphere endowed with normal vectors pointing outwards if $r > 0$, and inwards if $r < 0$. We introduce the Minkowski inner product and squared distance in $\mathbb{R}^4$ by letting

$$\langle\!\langle X_1, X_2 \rangle\!\rangle = x_1 x_2 + y_1 y_2 + z_1 z_2 - r_1 r_2 = X_1^T J X_2, \tag{2}$$

$$d^2(X_1, X_2) = \langle\!\langle X_1 - X_2, X_1 - X_2 \rangle\!\rangle, \quad \text{where } J = \operatorname{diag}(1, 1, 1, -1).$$

It is easy to see that $\sqrt{d^2(X_1, X_2)}$ is the tangential distance of spheres, measured between the contact points of a plane that is in oriented contact with both; see inset figure. Contact of oriented spheres is expressed by

$$d^2(X_1, X_2) = 0.$$

It is known that in this coordinate representation, a Laguerre transform acts as an affine mapping $X \mapsto \lambda A X + T$, where λ is a nonzero factor, $A \in \mathbb{R}^{4\times 4}$ is a matrix obeying $A^T J A = J$, and $T \in \mathbb{R}^4$.

2.1.2 Laguerre Transformations of Planes and Normal Vectors.
Planes are entities of Laguerre geometry, so a Laguerre transformation can be applied to them. It is known that parallel planes are mapped to parallel planes by a Laguerre transformation. It therefore makes sense to ask in what way Laguerre transforms act on normal vectors. It turns out that this action is that of a Möbius transform of the unit sphere S^2:

$$\begin{array}{ccc}
\{\text{planes}\} & \xrightarrow{\text{Laguerre transf.}} & \{\text{planes}\} \\
\downarrow & & \downarrow \\
\{\text{normal vectors}\} & \xrightarrow{\text{Möbius transf.}} & \{\text{normal vectors}\}
\end{array}$$

We describe a point (x, y, z) in $\mathbb{R}^3$ by homogeneous coordinates $X = (x_1 : x_2 : x_3 : x_4)$ where $x = \frac{x_1}{x_4}$, $y = \frac{x_2}{x_4}$, $z = \frac{x_3}{x_4}$. In these coordinates, the unit sphere is described by

$$X \in S^2 \iff X^T J X = 0, \text{ where } J = \operatorname{diag}(1, 1, 1, -1). \tag{3}$$

A Möbius transform of the unit sphere reads $X \mapsto AX$, where $A \in \mathbb{R}^{4\times 4}$ obeys $A^T J A = J$. The matrix A is the same as the one occurring in §2.1.1.

2.1.3 Laguerre Transforms of Smooth and Discrete Surfaces.
Applying a Laguerre transformation to the points of a smooth surface Φ, as well as to planes and spheres tangent to Φ, one gets spheres and planes tangent to a well-defined image surface Φ' [Cecil 1992].

As to meshes, Laguerre transformations act on the face planes. To recover the vertices of the transformed mesh we need to intersect face planes again. This procedure works only for special meshes, fortunately the conical meshes are among those [Liu et al. 2006]. We will be using Laguerre transforms later in this paper (see Figures 19, 24). Here we only mention that the passage from a mesh to an offset mesh at constant face-face distance is also an example of a Laguerre transform.

Laguerre transforms operating on surfaces are known to map principal curvature lines to principal curvature lines [Cecil 1992]. We will be concerned with surfaces where principal curvature lines are contained in planes. They, too are preserved:

PROPOSITION 2.1. *A Laguerre transformation maps a planar curvature line c to a planar curvature line c^* on the image surface.*

The proof makes use of the following form of Joachimsthal's theorem, see e.g. [do Carmo 1976, p. 152]:

PROPOSITION 2.2. *Consider the normal vector field $n(t)$ along a principal curvature line $c(t)$ in a surface. If the curve lies in a plane with normal vector e, then the angle $\sphericalangle(n(t), e)$ is constant. Conversely, existence of e with this property implies that the curve c lies in a plane.*

PROOF OF PROP. 2.1. If $n(t)$ are the unit normal vectors along $c(t)$, then Prop. 2.2 says that $n(t)$ traces out a circle in the unit sphere S^2. A Laguerre transform maps normal vectors by way of a Möbius transform, preserving circles. So the normal vector field $n^*(t)$ of $c^*(t)$ is a circle. Prop. 2.2 in reverse shows that c^* lies in a plane. □

2.2 Torsion-Free Support Structures

Pottmann et al. [2007] propose the term *torsion-free support structure* for a certain arrangement of planes along the edges of the mesh. The topic of the present paper represents a special case of this, namely one where many of the occurring planes are the same. We found that a more general look at torsion-free support structures yields insights valuable for our special case. Therefore the text below contains a theoretical discussion which first applies to a more general setting and only later is specialized to our case. Basically we introduce a certain version of homogeneous coordinates for the planes of a mesh from which we can read off geometric properties.

2.2.1 Torsion-free Support Structures and Their Weighted Face Images.
Consider a polyhedral mesh $M = (V, E, F)$. The plane carrying the face $f_i \in F$ has an equation of the form
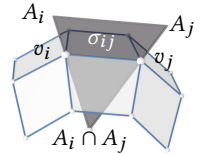
$$n_i \cdot x + d_i = 0,$$

where n_i is a normal vector. We consider the vector

$$f_i = \begin{bmatrix} n_i \\ d_i \end{bmatrix} \in \mathbb{R}^4 \tag{4}$$

as coordinates of this plane. It is unique up to a nonzero factor. Once the factor is chosen, f_i is called a *weighted plane*. It turns out that weighted planes allows us to formulate new properties of so-called torsion-free support structures. Following [Pottmann et al. 2007], we define:

Definition 2.3. A torsion-free support structure associated with M consists of a node axis A_i passing through each vertex v_i, and a supporting plane σ_{ij} for each edge $v_i v_j$ which contains both axes A_i and A_j. To avoid degeneracies we require that σ_{ij} does not contain the faces adjacent to the edge $v_i v_j$.

PROPOSITION 2.4 (*Definition and Properties of Weighted Face Image*). *Consider a simply connected polyhedral mesh M equipped with a torsion-free support structure where every edge $v_i v_j$ is associated with a support plane σ_{ij}. We require that neighbouring faces do not lie in the same plane. We can choose weighted plane coordinates f_j of faces and s_{ij} of supporting planes such that*
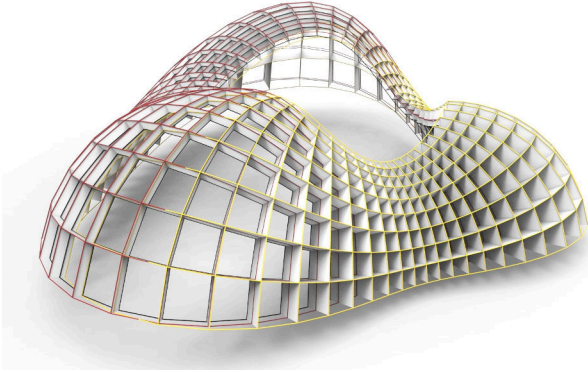
$$s_{ij} = f_r - f_l, \tag{5}$$

Fig. 4. Meshes are F-transforms if they share a support structure. Their respective face images are parallel meshes . Here three F-transforms (shown by yellow, red, and black edges) have been created by simply parallel translating the face image M_F of a base mesh M.

whenever the edge $v_i v_j$ is the intersection of faces f_l, f_r.

We now construct the weighted face image M_F of M as a combinatorial dual of M which is contained in $\mathbb{R}^4$. The coordinate vectors f_j of faces of M serve as vertices of M_F.

Then the faces of M_F are planar.

PROOF. Since the faces f_l, f_r and the edge plane σ_{ij} have a straight line intersection, we can achieve (5) locally for each edge, by multiplying plane coordinates with appropriate factors. We can also propagate (5) through a sequence of edges. Now consider the cycle of faces $f_1, \dots, f_k$ around a vertex v. Assume that (5) holds for all edges $f_i \cap f_{i+1}$, $1 \le i < k$. The planes $f_i - f_{i+1}$ associated with these edges contain the vertex v and in fact contain all points $v + \lambda a$ on the node axis passing through v. This amounts to 2 independent linear conditions imposed on the vectors $f_i - f_{i+1}$. The plane $f_1 - f_k$ by construction passes through the edge $f_1 \cap f_k$ and it obeys the aforementioned conditions, since

$$f_1 - f_k = (f_2 - f_1) + \cdots + (f_k - f_{k-1}).$$

Thus the plane $f_1 - f_k$ contains the node axis, and coincides with the support plane of the edge $f_1 \cap f_k$. This shows that propagation of Equ. (5) is consistent around each vertex, and, by simple connectedness, is consistent globally.

The eges of the dual face in M_F corresponding to v are given by vectors $f_i - f_{i+1}$ (indices modulo k). Because of the 2 linear conditions mentioned above, these edges lie in a two-dimensional plane. □

Given M_F, a torsion-free support structure is derived via Equ. (5). Scaling of M_F with a nonzero factor does not change the torsion-free support structure, but apart from that, M_F and the support structure determine each other uniquely:

PROPOSITION 2.5. *Consider a generic mesh $\widetilde{M}$ in $\mathbb{R}^4$ whose faces lie in 2D planes. Then there exists a mesh M equipped with a torsion-free support structure whose weighted face image equals $\widetilde{M}$.*

PROOF. The combinatorics of M are dual to those of $\widetilde{M}$. We directly read off the face planes of M from the corresponding dual vertices of $\widetilde{M}$. To reconstruct a vertex v from adjacent face planes

$f_1, \dots, f_k$, we must solve the linear system $(v, 1) \cdot (f_1, \dots, f_k) = 0$. The dimension 2 requirement generically implies a unique solution v; we appeal to genericity to avoid a discussion of cases. The edge vectors $f_1 - f_2, \dots$ correspond to planes that intersect in a straight line, because their span is 2-dimensional. Thus these coordinates correspond to the planes of a torsion-free support structure. □

2.2.2 The Weighted Normal Image of a Mesh. The weighted face image M_F of M is now used to construct the so-called weighted normal image M_N of M. This happens by forgetting the 4th coordinate, projecting M_F onto a mesh M_N in $\mathbb{R}^3$ which we call the *normal image* of M. Like M_F it is a combinatorial dual of M, and its faces are planar.

Note that the vertices of M_N are normal vectors, but not necessarily *unit* normal vectors. If they were, we would call M_N a *Gauss image*, in the tradition of differential geometry.

The auxiliary meshes M_F and M_N each have a particular purpose. Firstly, the mesh M_F serves to encode the support structure we endow the original mesh M with. Secondly, special properties of M like planar polylines will be expressed in terms of much better accessible properties of M_F. E.g. M has two families of planar polylines, if M_F is generated by translation (Prop. 3.1). The additional level of abstraction caused by M_F living in $\mathbb{R}^4$ is compensated by the now much easier access to the planar polylines property.

Properties involving *angles* can be read off the normal image M_N which lives in dimension 3. E.g. applications may demand a support structure orthogonal to the base mesh M. This is expressed by M_N being spherical (§2.3.2). Right angles in the support structure's nodes correspond to M_N being principal (§2.3.4). M_N is an important technical device in our extensive discussion of conical PP meshes (§4.1). Finally, for interactive design we need as many geometric transformations as possible that can be applied to support structures. These likewise can be derived from M_F (§§ 2.2.3, 2.3.5).

2.2.3 F-Transforms and Parallel Meshes. Polyhedral meshes M, M' with the same combinatorics are called F-transforms of each other, if corresponding edges e, e' are co-planar. They are called parallel meshes (Combescure transforms), if corresponding edges are even parallel [Bobenko and Suris 2008], see Fig. 4. In the architectural context M and M' are seen as a two-layer structure where the inner and outer surface have variable distance from each other [Pottmann et al. 2007]. In such a situation the planes carrying corresponding edges e, e' obviously constitute a torsion-free support structure for both M, M'. If M, M' are F-transforms of each other, Prop. 2.4 implies that the respective face images M_F, M'_F are parallel meshes.

2.3 Geometric Properties of Support Structures

In applications, geometric properties like the angle beween edges or the angle between planes often is an issue and corresponding constraints enter our design problem. This section discusses several such properties that might be imposed on torsion-free support structures.
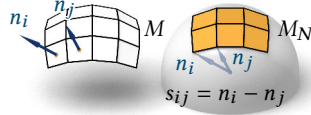
2.3.1 The Analogy between Discrete and Smooth Differential Geometry. In our discussion of geometric properties we are guided by the analogy between discrete and continuous objects, and we draw on known results from differential geometry. The analogies we use

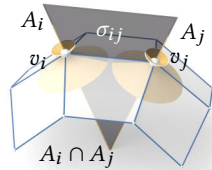in the immediately following paragraphs are summarized by the following table:

$$mesh \longleftrightarrow surface,$$
$$quad\ mesh \longleftrightarrow parametrization\ of\ surface,$$
$$quad\ mesh\ with\ planar\ faces \longleftrightarrow conjugate\ parametrization,$$
$$circular\ or\ conical\ mesh \longleftrightarrow principal\ parametrization.$$

These analogies assume fairness, i.e., the edges of meshes approximate first derivatives, and whenever 2nd order properties are concerned, we assume that 2nd order differences approximate 2nd derivatives. Under these assumptions, a quad mesh with planar faces approximates a conjugate parametrization, while the circular and conical properties imply that this parametrization is close to *principal* [Liu et al. 2006].

2.3.2 Right Angles Between Support Structure and Panels. The first property we study concerns the angle between support planes and panels. In applications this might be required to be close to 90 degrees. In the weighted normal image M_N, the normal vectors of these items are represented by dual edges resp. dual vertices — a dual vertex n_i here is interpreted as the vector $\overrightarrow{on_i}$ attached to the origin. We conclude: The right angle requirement is expressed by a *spherical* shape of M_N, because only then edges and vertices are orthogonal.

2.3.3 Principal Meshes — Conical and Circular Meshes. A mesh with planar faces is *conical*, if the faces adjacent to a vertex v_i touch a common cone of revolution. The axis A_i of this cone serves as node axis of a torsion-free support structure; the corresponding supporting planes σ_{ij} of edges are bisectors of adjacent faces [Liu et al. 2006]. These properties imply that the normal vectors n_i occurring in the weighted normal image M_N are unit vectors; this is because then

$$s_{ij} = n_i - n_j$$

computes exactly the normal vector of the bisecting support plane. Thus M_N is inscribed in the unit sphere. Faces of M_N are planar and so have circumcircles; we conclude M_N is a circular mesh.

Remark 2.1. A principal curvature line parametrization of a surface can be discretized in several ways, and it seems a bit arbitrary to prefer the conical meshes over other choices, e.g. circular meshes. However it typically does not matter which version of principal meshes we use. By choosing one particular property, say, the conical property, we will not lose generality as far as approximation of the continuous situation is concerned.

2.3.4 Right Angles in Nodes. After the preparations in § 2.3.3, we turn to another property imposed on torsion-free support structures, namely a near-orthogonal intersection of supporting planes. This question does not concern M itself, it addresses only the support structure associated with it. We say such a support structure has *orthogonal nodes*.

Interestingly, this property means that the weighted normal image M_N is principal. To see this, observe that orthogonality of support
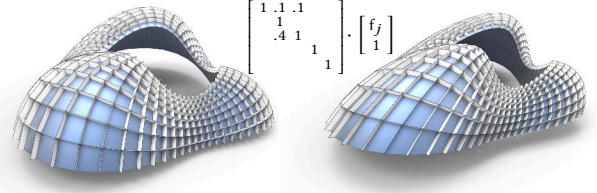

Fig. 5. The mesh and torsion-free support structure at left is being modified by applying a projective mapping in 4-space to its weighted face image M_F. After introducing homogeneous coordinates, this transformation is expressed by multiplication with a matrix.

planes means orhogonality of their respective normal vectors. These normal vectors occur as edges of M_N, so edges of M_N are approximately orthogonal. M_N already has planar faces, and the additional orthogonality property now means it is principal. We are free to impose any of the available properties expressing principality. In this particular case it is convenient to require that M_N is a circular mesh.

2.3.5 Transformations of Torsion-Free Support Structures. It is an old geometer's trick to transfer objects from one space to another in order to benefit from the latter's transformations. The following paragraphs describe how this idea can be applied to torsion-free support structures

We may subject a mesh M with torsion-free support structure to projective transformations without destroying the support structure property. The group of projective transformations of 3-space is 15-dimensional. However, transfer to the face image M_F via Prop. 2.4 yields a mesh in 4-dimensional space and a much greater set of transformations: applying a 4D projective transformation (with its 24 degrees of freedom) to M_F does not destroy the relevant properties. We can then employ Prop. 2.5 and turn the transformed face image back into a mesh plus support structure — see Fig. 5.

Remark 2.2 (Isotropic Möbius Transforms for Support Structures with Orthogonal Nodes). In § 2.3.4 we discussed support structures with orthogonal nodes – they were characterized by M_N being circular. An alternative characterization is that the face image M_F projects onto a circular mesh M_N when we forget the 4th coordinate.

There is a 16-dimensional group of *isotropic Möbius transformations* in 4-space which preserve the property of four points "lying in a plane and projecting onto a circular quad". Any such transformation can be applied to M_F without destroying the right-angled
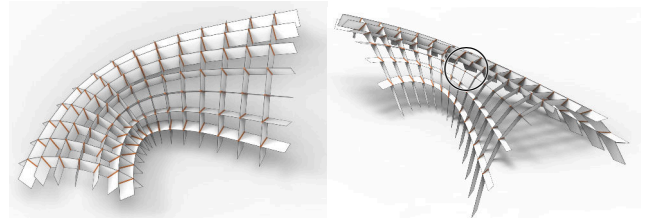

Fig. 6. Support structures with orthogonal nodes. These two support structures are connected by an isotropic Möbius transform acting on their respective 4D circular face images M_F, M_F'. The orthogonal nodes property is visible only for such nodes where the axis is a projecting ray.

node property. Fig. 6 shows an example. For the formulae we refer to [Pottmann and Peternell 1998].

3 MESHES WITH PLANAR SUPPORTING BEAMS

3.1 P-Meshes and PP-Meshes

This section introduces the P and PP properties which are the main focus of this paper. All involved meshes are *polyhedral*, i.e., they have planar faces.

3.1.1 Definition of the P and PP Property. Consider a polyhedral quad mesh which locally has the combinatorics of a regular grid. Vertices $v_{i,j}$ are indexed by integers i, j. We call it a P-mesh, if there is a sequence of planes U_i such that

$$v_{i,j} \in U_i \quad \text{for all } i, j,$$

that is, one family of mesh polylines is planar. We could just as well have required existence of planes W_j such that $v_{i,j} \in W_j$. The mesh is called a PP mesh, if there are planes U_i and W_j such that

$$v_{i,j} \in U_i \cap W_j, \quad \text{for all } i, j.$$

In a PP mesh all mesh parameter lines are planar. The planes carrying parameter lines can be taken as part of a support structure.

For the following considerations we are indexing faces by their lowest corner, so that the vertices of the face $f_{i,j}$ are $v_{i,j}$, $v_{i+1,j}$, $v_{i+1,j+1}$, $v_{i,j+1}$.

We construct the weighted face image M_F according to §2.2.1. It has vertices $f_{i,j}$. Planes U_i and W_j are *support planes* in the sense of §2.2.1. According to Equ. (4) and Prop. 2.4, the cooordinates of support planes occur as edges of M_F. Thus the P-mesh condition translates to

$$f_{i,j+1} - f_{i,j} = \lambda_{i,j} u_i,$$

where u_i is the homogeneous coordinate vector of the plane U_i. Geometrically, this means that faces of M_F are trapezoids. For a PP mesh, we also have

$$f_{i+1,j} - f_{i,j} = \mu_{i,j} w_j,$$

where w_j are coordinates of planes W_j. The faces of M_F are parallelograms. This means that M_F is a discrete translation net.

In the PP mesh case, edges $\lambda_{i,j} u_i$ depend only on the index i, and edges $\mu_{i,j} w_j$ depend only on the index j. By relabelling these vectors u_i and w_j, respectively, we get

$$f_{i+1,j} - f_{i,j} = u_i, \quad f_{i,j+1} - f_{i,j} = w_j. \tag{6}$$

We have shown:

PROPOSITION 3.1. *If a mesh M has the P property, its face image M_F has faces that are trapezoids. If M has even the PP property, the faces of M_F are parallelograms, and thus M_F is generated by translating one mesh parameter line along a transverse mesh parameter line.*

3.1.2 Construction of P-Meshes and PP-Meshes from Initial Values. Computing PP meshes can be reduced to the problem of finding vertices v_{ij} constrained to lines $l_{ij} = U_i \cap W_j$ (this idea can also be used for computing P-meshes, where lines $l_{ij} \subset U_j$ are variables, and has been employed by Mesnil et al. [2017]). Once the lines l_{ij} are fixed, vertices can be uniquely propagated from Cauchy initial
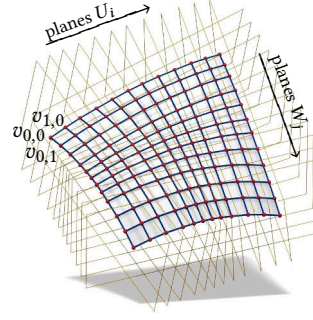

Fig. 7. Theoretical construction of a PP mesh from Cauchy initial data, if planes planes $U_0, U_1, \ldots$ and $W_0, W_1, \ldots$ are given. The vertex $v_{i+1,j+1}$ is found from $v_{i,j}$, $v_{i,j+1}$, $v_{i+1,j}$ by intersecting the plane spanned by these three vertices with the straight line $U_{i+1} \cap W_{j+1}$.

values, say, $v_{i,0}$ and $v_{0,j}$, see Fig. 7. It is however difficult to control the final shape via those initial values.

Equation (6) immediately implies that

$$f_{i,j} = f_{i,0} + f_{0,j} - f_{0,0}. \tag{7}$$

This yields an explicit dependence of vertices on Cauchy initial data. Geometric modelling based on (7) is much more stable than intersecting lines and planes, which is likely to even break down when the sign of Gaussian curvature changes. However it requires to appropriately initialize weighted plane coordinates at the boundary. We deal with the actual geometric design in §3.2.

3.1.3 Relation of PP Meshes to Bisector Surfaces. The statement of Prop. 3.1 refers to plane coordinates in dual space, and we want to give an interpretation in terms of primal space. Equation (7) can be rewritten as

$$f_{i,j} = g_i - h_j,$$

e.g. by letting $g_i = f_{i,0}$ and $h_j = f_{0,0} - f_{0,j}$. Now we interpret g_i and h_j as coordinates not of planes, but of *spheres*, where a vector $g = (g_1, g_2, g_3, g_4) \in \mathbb{R}^4$ corresponds to the sphere Σ_g with equation $\|x\|^2 + (g_1, g_2, g_3)^t \cdot x + g_4 = 0$. With another sphere Σ_h corresponding to $h \in \mathbb{R}^4$, we consider the *radical plane* associated with Σ_g, Σ_h. Its equation is the difference

$$\left((g_1, g_2, g_3)^T - (h_1, h_2, h_3)^T \right) \cdot x + (g_4 - h_4) = 0$$

of equations of Σ_g, Σ_h. This plane passes through the intersection $\Sigma_g \cap \Sigma_h$. In the special case of zero radius, both Σ_g and Σ_h are reduced to points, and the radical plane is the bisector plane. Observe that the coordinates of the radical plane is just $g - h$, so we can say that the weighted face image consists of the radical planes of spheres Σ_{g_i} and spheres Σ_{h_j}.

The reason we invoke this interpretation is that it leads to a geometrically interesting special case of PP meshes: With a polyline of zero-radius spheres g_i and another such polyline h_j, the definition $f_{i,j} = g_i - h_j$ yields the weighted face image of a PP mesh whose face planes bisect the given two polylines; see Figure 8. The PP mesh can therefore be considered as a discrete bisector surfaces of two polylines.

A change in the radius of the involved spheres changes the 4-th coordinate in vectors g_i and h_j, but not the normal vectors of the planes f_{ij} which are represented by coordinates 1,2,3. Thus changing the radii means that the PP mesh constructed in this way is replaced
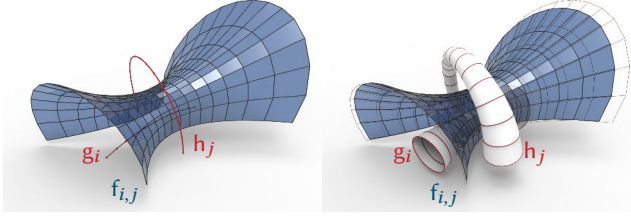
Fig. 8. PP meshes as bisector surfaces. At left, the face planes $f_{i,j}$ of a PP mesh M are bisecting the vertices of two polylines g_i and h_j which are actually spheres of zero radius. At right, these vertices swell and become true spheres. Then bisector planes become radical planes, and M is replaced by a parallel mesh. We visualize the sphere g_i by means of a channel surface tangent to them, and the same for h_j.

by a parallel mesh. The analogous continuous construction was proposed by Darboux [1896].

Remark 3.1. Bisectors have been studied by [Elber and Kim 1998; Peternell 2000], mainly from an algebraic perspective. The PP property is not mentioned, but is already apparent in simple cases: the bisector of two straight lines is a hyperbolic paraboloid, which has parabolas as planar + conjugate parameter lines. Similarly, the superclyde occurring as a bisector of two circles [Peternell 2000] features conics as parameter lines.

Remark 3.2 (*The Multi-Net Property of PP Meshes*). The explicit representation of (7) shows the following: When we delete an entire row of dual vertices in M_F and recompute the base mesh M by intersecting the remaining face planes, we get a PP mesh again. The same is true for columns. This is a dual version of the *multi-net property* which is the subject of [Bobenko et al. 2020].

3.2 Interactive Editing of PP Meshes

3.2.1 *The Principle of Design by Tangent Planes.*
The geometric design of PP quad meshes is based on Proposition 3.1 and the explicit representation of vertices $f_{i,j}$ of the weighted face image by Equ. (7). For design purposes it will be good to think of the face coordinates
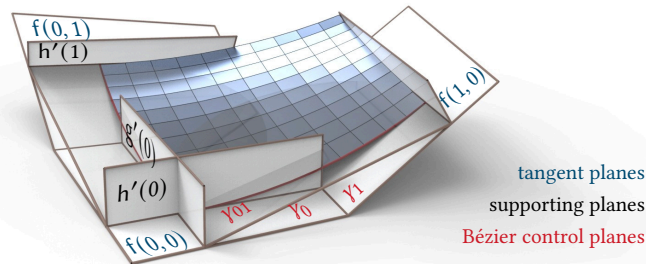

Fig. 9. A surface $x(u, v)$ with the PP property is constructed as envelope of its tangent planes $f(u, v) = g(u) + h(v) - c$. The supporting planes of the u and v parameter lines are given by partial derivatives $f_v = h'(v)$ and $f_u = g'(u)$, respectively. Labels $\gamma_0, \gamma_{01}, \gamma_1$ identify control elements discussed later.
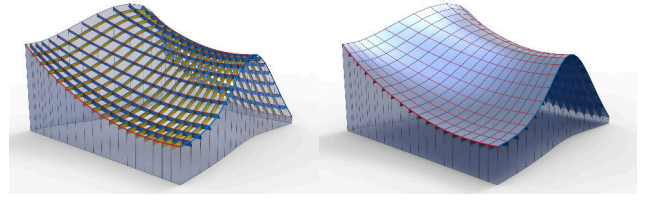
Fig. 10. A PP mesh whose weighted face planes $f_{i,j}$ are samples of a smooth dual surface $f(u, v)$. We here show the support structure of the mesh, and the primal surface $x(u, v)$ derived from $f(u, v)$ according to Equ. (9).

$f_{i,j}$ as discrete samples of smooth functions:

$$f_{i,j} = f(u_i, v_j), \text{ where } f(u, v) = \underbrace{f(u, 0)}_{=: g(u)} + \underbrace{f(0, v)}_{=: h(v)} - \underbrace{f(0, 0)}_{=: c}. \quad (8)$$

Note that $g(0) = h(0) = c$. The continuous surface $x(u, v)$ whose tangent planes are $f(u, v)$ is reconstructed by intersecting $f(u, v)$ with partial derivatives f_u, f_v. We symbolically write

$$x(u, v) = f \times f_u \times f_v = (g(u) + h(v) - c) \times g'(u) \times h'(v). \quad (9)$$

The prime indicates derivatives. We see that all points of the v parameter line $x(u_0, v)$ are contained in the plane $g'(u_0)$; it is a *support plane* of this parameter line. Likewise, $h'(v_0)$ is the supporting plane of the u parameter line $x(u, v_0)$ — see Fig. 9.

The PP mesh whose face planes $f_{i,j}$ are samples of $f(u, v)$ has the very same support planes $g'(u_i)$ and $h'(v_j)$. Note that the vertices of the mesh are not samples of the surface $x(u, v)$; the sample property applies to planes.

Example. Fig. 10 illustrates a simple case of interactive design based on this approach. Given are curves $c(u)$ (red, contained in a plane ε) and $d(v)$ (blue, contained in a plane φ). With $m(u), n(v)$ as unit normal vectors of these curves within ε, φ, resp., we let $f(u, v) = \left[\begin{smallmatrix} m(u) + n(v) - m_0 \\ m_0 \cdot c_0 - m(u) \cdot c(u) - n(v) \cdot d(v) \end{smallmatrix} \right]$. It is easy to check that the surface $x(u, v)$ constructed via Equ. (9) interpolates both curves, if some conditions are met: ε, φ are orthogonal, the curves meet in a common point $c_0 \in \varepsilon \cap \varphi$ and have a common normal vector m_0 there. A PP mesh is derived from $f(u, v)$ by sampling. We have thus reduced the interactive design of PP meshes to the interactive design of 2D curves.

3.2.2 *A Bézier Curve Approach to Geometric Design of PP Meshes.*
Geometric modelling based on Equations (8) and (9) hinges on the choice of curves $g(u)$ and $h(v)$ which lie in $\mathbb{R}^4$ and are not accessible visually. We show how to nevertheless perform geometric modeling via controls that can be interactively handled by the user. We use a curve $g(u)$ which is the concatenation of quadratic segments $g^{(0)}, g^{(1)}, \ldots$ Each segment is determined by control points $g_i, g_{i,i+1}, g_{i+1}$:

$$g^{(i)}(u) = (1-u)^2 g_i + 2u(1-u) g_{i,i+1} + u^2 g_{i+1} \quad (0 \le u \le 1).$$

Fig. 11 shows an example. It is easy to verify that the segments fit together in a tangent-continuous way if and only if points

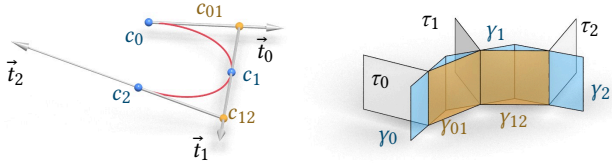$$g_{i-1,i}, \ g_i, \ g_{i,i+1} \quad (10)$$

Fig. 11. *Left:* Control points $c_0, c_{01}, c_1, \ldots$ for a spline curve consisting of segments $c^{(0)}(t), c^{(1)}(t), \ldots$ which fit togeher with tangent continuity. We also indicate vectors $\vec{t}_i$ indicating the direction of the curve when passing through the point c_i. *Right:* Analogous control structure $\gamma_0, \gamma_{01}, \gamma_1, \ldots$ for a spline in plane space. In our setting, the planes τ_i related to the spline's tangents serve as support planes and are intuitive handles for modeling.

are lying on a straight line, in that order (if the order is reversed, the union of segments has a cusp). Similarly the curve $h(v)$ is defined by control points $h_0, h_{01}, \ldots$ To meet the requirement that $g(0) = h(0)$, we choose $g_0 = h_0$, but otherwise curves g, h are independent from each other.

For the actual design, we cannot expect the user to select control elements $g_0, g_{01}, g_1, \ldots$ in the four-dimensional space of weighted planes. Instead, the user picks an arrangement of planes $\gamma_0, \gamma_{01}, \gamma_1, \ldots$ as shown in Fig. 11, right. If weighted plane coordinates are to obey (10), the corresponding planes

$$\gamma_{i,i-1}, \ \gamma_i, \ \gamma_{i,i+1}$$

must intersect in a common line. The user also chooses a plane τ_i passing through that same line which eventually serves as a supporting plane of the generated PP mesh.

To reconstruct a tangent-continuous union of curve segments from these data, we choose weighted plane coordinates $\bar{g}_i, \bar{g}_{i,i+1}, \bar{t}_i$ for planes $\gamma_i, \gamma_{i,i+1}, \tau_i$, respectively. We then find control points as required by a recursive re-weighting procedure. We let $g_0 := \bar{g}_0$ and solve

$$g_0 + \mu_0 \bar{t}_0 = \lambda_{01} \bar{g}_{01}, \qquad g_{01} := \lambda_{01} \bar{g}_{01}$$
$$g_{01} + \nu_0 \bar{t}_0 = \lambda_1 \bar{g}_{01}, \qquad g_1 := \lambda_1 \bar{g}_1$$

(with unkonwn coefficients $\mu_i, \nu_i, \lambda_i, \lambda_{i,i+1}$), and so on for $g_{12}, g_2, \ldots$ The control points computed in this way define curve segments fitting together to form the tangent-continuous curve $g(u)$. It is constructed such that the derivatives at the endpoints of segments correspond to the plane coordinates of planes τ_i.

Since the arrangement of planes in Fig. 11 has quite a lot of constraints, we assist the user by setting up a procedure to interactively modify the arrangement, while side-conditions are maintained by

Fig. 13. A design with planar faces exhibiting the PP property made by the spline method described by §3.2.2.

an optimization running in the background. We do not describe the details here, since we do not regard it as a contribution of the present paper — see Fig. 12 and accompanying video.

An analogous procedure yields the curve $h(v)$. Together, using the explicit expressions given at the top of this section, they define a dual surface $f(u, v)$ and, by sampling that, a PP mesh. Note that the support planes of this PP mesh are given by the derivatives of curves g, h. This is why we made those support planes a design handle.

Remark 3.3. Recall that the dual curve $g(u)$ is tangent-continuous only if control points $g_{i-1,i}, g_i, g_{i,i+1}$ lie on a straight line, in that order. It is not difficult to see that this condition is fulfilled if and only if planes $\gamma_{i-1,i}, \gamma_i, \gamma_{i,i+1}, \tau_i$ are arranged in that order, as shown by Fig. 11. This is not the case for the nonconvex example of Fig. 12, and indeed the curve $g(u)$ features a cusp here. The user does not notice this phenomenon which happens in the space of weighted planes.

3.3 Computing P Meshes by Optimization

The P property — planarity of only 1 family of mesh parameter lines — is a comparatively mild restriction. We found it quite easy to establish by optimization, provided we start from a mesh with planar faces already optimized for use in freeform architecture (using e.g. the method of Tang et al. [2014]). Their mesh polylines are smooth to such an extent that we experienced no obstacles in imposing the P property in addition to planarity of faces. Figures 14 and 25 show examples. The process is the following. We consider a mesh (V, E, F) with a collection S of supporting planes. Variables in optimization are vertices $v \in V$, and unit normal vectors n_f, n_σ of all faces $f \in F$ and of supporting planes $\sigma \in S$. By summation over all edges vw
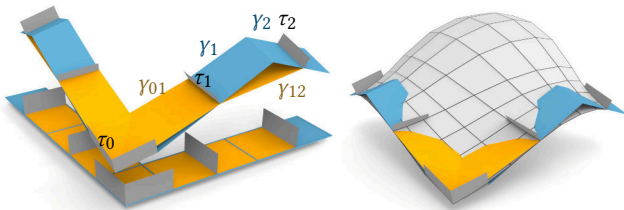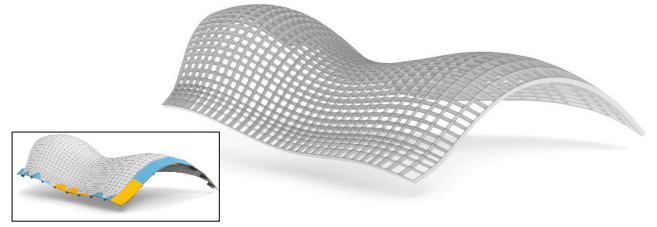

Fig. 12. Interactive modeling with the control structure for PP meshes. *Left:* Initial position and user-modified position of the control elements. *Right:* A PP mesh derived from those.
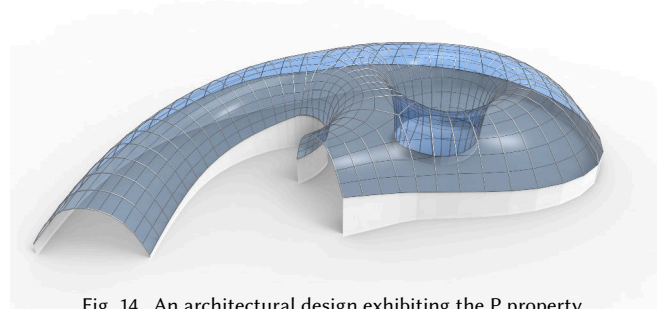

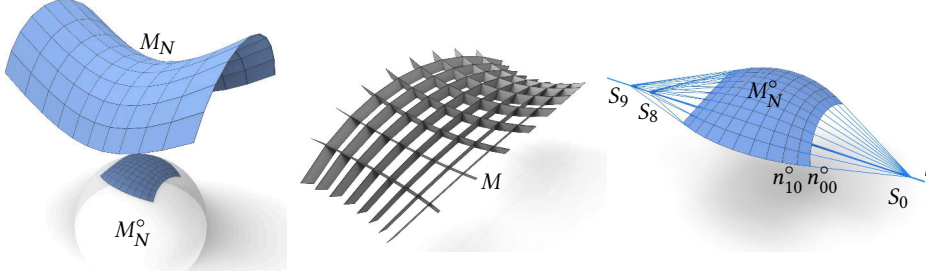
Fig. 14. An architectural design exhibiting the P property.

Fig. 15. A conical mesh M with planar parameter lines has two weighted normal images, namely a translation net M_N and a circular mesh M_N° which is the projection of M_N onto the unit sphere. Prop. 4.1 describes how the vertices n_{ij}° of M_N° arise by sampling two orthogonal pencils of circles in the unit sphere.

contained in the planes mentioned, we build energies

$$E_P = \sum_{\sigma \in S} \sum_{vw \in \sigma} \langle n_\sigma, v - w \rangle^2, \qquad E_f = \sum_{f \in F} \sum_{vw \in f} \langle v - w, n_f \rangle^2,$$

which penalize deviation from those planes. We use the energy

$$E_1 = \sum_{\sigma \in S} (\|n_\sigma\|^2 - 1)^2 + \sum_{f \in F} (\|n_f\|^2 - 1)^2$$

to force normal vectors to be of length 1. We also employ a fairness energy $E_{\text{fair}} = \sum_{\text{triples } uvw} \|(u - v) - (v - w)\|^2$, where summation is over all successive vertices of mesh polyline where fairness is to be imposed. The total energy $\lambda_P E_P + \lambda_f E_f + \lambda_1 E_1 + \lambda_{\text{fair}} E_{\text{fair}}$ has been minimized using a Levenberg-Marquardt method [Madsen et al. 2004]. Figures 14 and 25 show results of this optimization.

For the examples produced in this paper, we let $\lambda_{\text{fair}} = 0.01$ and $\lambda_P = \lambda_f = \lambda_1 = 1$. To evaluate the quality of results, we measure planarity of a face f by the distance δ_f of diagonals divided by average length of diagonals. Planarity of a mesh polyline P is expressed by the value δ_P which is the maximum distance of P's vertices from a best approximating plane, divided by the bounding box diameter of P. We summarize the results of optimization:

	max. δ_P	avg. δ_P	max. δ_f	avg. δ_f
Fig. 14	$1.6 \cdot 10^{-5}$	$2.8 \cdot 10^{-6}$	$1.4 \cdot 10^{-5}$	$1.7 \cdot 10^{-6}$
Fig. 25	$1.2 \cdot 10^{-4}$	$2.9 \cdot 10^{-5}$	$1.4 \cdot 10^{-4}$	$2.3 \cdot 10^{-5}$

We do not consider this optimization a major result of the present paper, since it is very similar to other cases where global optimization of meshes is employed.

4 PRINCIPAL MESHES WITH THE P AND PP PROPERTY

In architectural design, a highly visible property is that of orthogonal or near-orthogonal intersection of edges, or the near-rectangular shape of planar panels. This leads to so-called *principal meshes*, see §2.3.3. Our focus is on meshes enjoying the P or even the PP property. Among different definitions of principal meshes, we choose to work with *conical* meshes. This is because then we can treat the P and PP properties elegantly via the Laguerre geometry of planes.

Recall the definition and properties of a *conical mesh* from § 2.3.3, in particular the torsion-free support structure canonically associated with it. Recall also the weighted normal image of a mesh in §2.2.2. The weighted normal image and face image associated with the canonical support structure will be labelled M_N° and M_F°, respectively. M_N° is inscribed in the unit sphere (see Fig. 15).

If M is endowed with another torsion-free support structure (e.g., if M enjoys the PP property), another face image M_F and normal vector image M_N are derived from it. Since the base mesh M is still the same, corresponding vertices of M_F and M_F° are proportional,

and so are corresponding vertices of M_N and M_N°. Thus M_N° arises from M_N by normalization, i.e., projection to the unit sphere, see Fig. 15. Similarly M_F° arises from M_F by a projection which normalizes the first three coordinates. The existence of these projections is a strong constraint on the geometry of M_F and M_N, since planarity of faces must not be destroyed by the projection.

Fig. 15 shows the two different weighted normal images M_N, M_N° asssociated with such a mesh M. The conical property allows us to derive one support structure, the PP property leads to another. The former leads to M_N° inscribed in the unit sphere, the latter leads to M_N which is a translational net.

4.1 Conical PP Meshes

The conical condition on top of the PP property is very restrictive. It is in general not achievable by optimization — see the discussion around Fig. 23. An example where we nevertheless succeeded is shown by Fig. 16. Here optimization started from a conical mesh which is the union of patches, each of which enjoys regular grid combinatorics. We managed to optimize this mesh so that all the short polylines contained in individual patches become planar (in the notation of §3.3, we achieved $\delta_f = 10^{-7}$, $\delta_{P,\max} = 2.6 \cdot 10^{-6}$, $\delta_{P,\text{average}} = 3.3 \cdot 10^{-7}$).

For design we use a different approach based on an explicit description of the shapes of achievable meshes. The weighted normal images M_N, M_N° mentioned in the previous paragraph can be described completely (see Cases 1,2 below). Degrees of freedom available for design are only contained in the 4th coordinate of the weighted face image which is not yet determined by the weighted normal image.

The continuous analogue of a conical PP mesh is a surface all of whose curvature lines are planar. Recall that the surface intersects the plane carrying a curvature line under a constant angle (Prop. 2.2). Orthogonality then implies that the Gauss image must be rather special: There are two pencils of planes (with their axes being polar to each other) which intersect S^2 in exactly the circles mentioned above.

The discrete version of such a situation has been studied to a certain extent [Mesnil et al. 2018; Tellier 2020; Tellier et al. 2019]. We extend this work by proving the following statement which is also illustrated by Fig. 15.

PROPOSITION 4.1. *Consider a conical quad mesh M of regular grid combinatorics that in addition enjoys the PP property. M_N°, M_N shall be the weighted normal images derived from these properties.*

Then there are two straight lines $l, \bar{l}$ which are polar w.r.t. the unit sphere S^2, and planes $\alpha_i \supset l, \bar{\alpha}_j \supset \bar{l}$, such that the vertices $n_{i,j}^\circ$ of M_N°

are contained in $\alpha_i \cap \bar{\alpha}_j$. In particular the mesh parameter lines of M_N° lie on circles contained in planes α_i resp. $\bar{\alpha}_j$.

PROOF. The proof uses projective geometry, for which we refer e.g. to [Berger 1987, §14.5]. We first establish a geometric fact concerning the projection of a parallelogram $pqrs$ onto a quad $p^\circ q^\circ r^\circ s^\circ$ in S^2. Firstly p, q, p°, q° lie in the 2D subspace $[p,q]$, so the straight line $p^\circ \vee q^\circ$ intersects the 1D subspace $[q-p]$ in a point S_{pq}, possibly at infinity. Since edges pq and rs are parallel, $[q-p] = [p,q] \cap [r,s]$. If vertices $p^\circ, q^\circ, r^\circ, s^\circ$ happen to be contained in a plane β, then obviously $S_{pq} = [p,q] \cap [r,s] \cap \beta$. This expression remains the same if edges pq and rs are exchanged, so $S_{rs} = S_{pq}$. If $pqrs$ shares the edge rs with another parallelogram $rsuv$ with analogous properties, the same argument shows that $S_{pq} = S_{rs} = S_{uv}$.

We apply this construction inductively to a row of parallelogram faces of M_N. Since M_N° has planar faces, all lines $\{n_{i+1,j}^\circ \vee n_{i,j}^\circ\}_{j \in \mathbb{Z}}$ meet in a common point S_i, see Fig. 15. Similarly, lines $\{n_{i,j+1}^\circ \vee n_{i,j}^\circ\}_{i \in \mathbb{Z}}$ meet in a common point $\bar{S}_j$.

It is known that for a quad $n_{i,j}^\circ, n_{i+1,j}^\circ, n_{i+1,j+1}^\circ, n_{i,j+1}^\circ$, inscribed in a circle, the intersection points $S_i, \bar{S}_j$ of opposite edges are conjugate. So $S_i, \bar{S}_j$ are conjugate also w.r.t. the unit sphere, i.e., S_i lies in the polar plane of $\bar{S}_j$. Since a single S_i lies in many such polar planes (one for each j), such a configuration is only possible if there is a straight line l carrying all S_i's. Reversing the argument, the points $\bar{S}_j$ lie on the straight line $\bar{l}$ polar to l.

Looking back, we have established that $n_{i,j+1}^\circ$ lies in the plane spanned by $n_{i,j}^\circ$ and l (because $S_i \in l$), and so does $n_{i,j-1}^\circ$ (because $S_{i-1} \in l$). By recursion, the entire parameter line $\{n_{i,j}\}_{j \in \mathbb{Z}}$ is contained in that plane, which is labelled α_i. Similarly each parameter line $\{n_{i,j}\}_{i \in \mathbb{Z}}$ is contained in plane $\bar{\alpha}_j$. □

Remark 4.1. The polar dual $(M_N^\circ)^*$ of M_N° w.r.t. the unit sphere is combinatorially equivalent to M, and its faces are, by polarity, parallel to the faces of M. Therefore we may recover M as a parallel mesh of $(M_N^\circ)^*$. Our design methods are not based on this approach, though.

4.1.1 Explicit Computation of Conical PP Meshes. As to the relative position of lines $l, \bar{l}$ which occur in Prop. 4.1, there are two cases:

Case (1) One of $l, \bar{l}$ is outside of the unit sphere S^2, the other one intersects S^2 in two points. The circles carrying the mesh's parameter lines form a pair of orthogonal pencils. This is the situation shown by Fig. 15.

Case (2) The lines $l, \bar{l}$ both touch S^2 in the same point, while being orthogonal. The circles carrying the mesh parameter lines of M form a pair of orthogonal "parabolic" pencils.

We start with case (1) and determine the possible weighted normal images M_N as shown by Fig. 15. We use a coordinate system adapted to the lines $l, \bar{l}$ such that they are given by the following equations:

$$l : x_2 = d, x_3 = 0, \quad \bar{l} : x_1 = 0, x_2 = 1/d, \quad \text{where } d > 1.$$

The 2D subspaces $\varepsilon, \bar{\varepsilon}$ spanned by $l, \bar{l}$ are the $x_1 x_2$ plane resp. the $x_2 x_3$ plane.
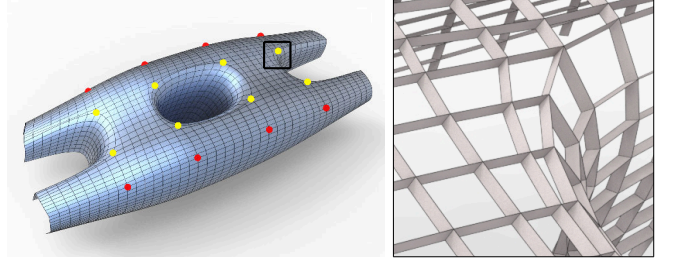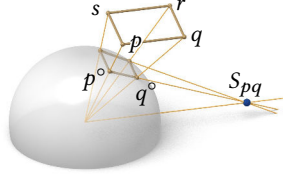

Fig. 16. A smooth union of conical PP meshes, each of which exhibits regular combinatorics, with combinatorial singularities (yellow) occurring only at corner vertices of individual PP patches. The detail at right shows the torsion-free support structure associated to the individual PP pieces.

The faces of M_N are parallelograms, and by the proof of Prop. 4.1 its edges are parallel to either ε or $\bar{\varepsilon}$. The parameter lines of M_N therefore lie in planes parallel to either ε or $\bar{\varepsilon}$, and we have

$$n_{i,j} = \begin{bmatrix} \varphi_1(u_i) \\ \varphi_2(u_i) \\ 0 \end{bmatrix} + \begin{bmatrix} 0 \\ \psi_2(v_j) \\ \psi_3(v_j) \end{bmatrix}.$$

The usage of functions $\varphi_1, \dots \psi_3$ indicates that we wish to represent the vertices of the mesh M_N as discrete sample of a continuous parametric surface. This is already known to be possible for the projection M_N°, because its parameter lines lie on circles. Backprojection into the aforementioned planes yields *conics* the parameter lines of M_N are samples of. An elementary calculation reveals that

$$n_{i,j} = n(u_i, v_j), \quad \text{where } n(u,v) = \begin{bmatrix} e \sin u \\ d \cos u + \cosh v \\ e \sinh v \end{bmatrix}, \quad e = \sqrt{d^2 - 1}.$$

This representation has already been given by [Blaschke 1929]. The plane image M_F in $\mathbb{R}^4$ has parallelogram faces like M_N, so it reads

$$f_{i,j} = f(u_i, v_j), \quad f(u,v) = \begin{bmatrix} n(u,v) \\ g(u) + h(v) \end{bmatrix}, \tag{11}$$

where g, h are arbitrary. As $d \to \infty$ we achieve a rotationally symmetric case:

$$f_{i,j} = f(u_i, v_j), \quad f(u,v) = \left(\sin u, \cos u, \sinh v, g(u) + h(v) \right)^T. \tag{12}$$

The mesh M_N then lies in a cylinder with rotational symmetry about the x_3 axis.

In case (2) we use a similar computation. We choose $l, \bar{l}$ as lines parallel to the x_1 and x_2 axis which are tangent to the unit sphere in the north pole. The result is

$$f_{i,j} = f(u_i, v_j), \quad f(u,v) = \left[u, v, \frac{u^2 + v^2 - 1}{2}, g(u) + h(v) \right]^T. \tag{13}$$

Apparently M_N is inscribed in the paraboloid $2x_3 = x_1^2 + x_2^2 - 1$. The parameter lines are samples of parabolas contained either in planes $x_1 = u_i$ or in planes $x_2 = v_j$. Projection onto S^2 yields the circles carrying the mesh parameter lines of M_N°.

4.1.2 A Representation of Conical PP meshes Adapted for Geometric Design. Representations (11) and (13) show that the face planes of a conical PP mesh are samples of a 2D continuous family $f(u,v)$. The envelope of this family of planes is a continuous surface $x(u,v)$

approximating the mesh. It depends on the lines $l, \bar{l}$ and on the functions g, h. The choice of $l, \bar{l}$ amounts to specifying the size and position of $x(u, v)$, while functions g, h determine its shape.

Using homogeneous coordinates $(x_1 : \ldots : x_4)$ corresponding to Cartesian coordinates $\frac{1}{x_4}(x_1, x_2, x_3)$, this envelope is computed via the 3-ary cross product of $f(u, v)$ with its partial derivatives, namely $x(u, v) = f \times f_u \times f_v$ – see Appendix.

Choosing the functions $g(u), h(v)$ is not a task that can be left to the designer. There is unfortunately no good intuitive relation between g, h on the one hand, and the geometric shape of the mesh on the other hand. In order to gain better insight into the right choices, and to find a path towards a design tool, we re-parameterize both $f(u, v)$ and $n(u, v)$, starting with Case 1.

We first observe that $n(u, 0) = (e \sin u + 1, d \cos u, 0)$ is an ellipse with focal point in the origin. It has the polar coordinate representation

$$(r(\varphi) \cos \varphi, r(\varphi) \sin \varphi, 0) \quad \text{with} \quad r(\varphi) = \frac{e^2(\sin \varphi + d)}{e^2 + \cos^2 \varphi}.$$

Likewise, $n(0, v)$ is a hyperbola. It is contained in the $x_2 x_3$ plane and has the polar coordinate representation

$$(0, s(\psi) \cos \psi, s(\psi) \sin \psi) \quad \text{with} \quad s(\psi) = \frac{e^2(d \cos \psi + 1)}{e^2 \cos^2 \psi - \sin^2 \psi}.$$

Note that we obtain the entire hyperbola as ψ ranges from 0 to 2π. The points at infinity are attained if $\tan^2 \psi = e^2$.

The weighted normal image $n(u, v)$ is symmetric w.r.t. the horizontal $x_1 x_2$ plane containing the ellipse, and is also symmetric w.r.t. the $x_2 x_3$ plane containing the hyperbola.

Using φ, ψ as parameters to substitute u and v, we obtain

$$\widetilde{n}(\varphi, \psi) = \begin{bmatrix} r(\varphi) \cos \varphi \\ r(\varphi) \sin \varphi + s(\psi) \cos \psi - d - 1 \\ s(\psi) \sin \psi \end{bmatrix}.$$

We have used that $r(\pm \pi/2) = d \pm 1$ and $s(0) = 1 + d$, $s(\pi) = 1 - d$. The above-mentioned ellipse and hyperbola are recoved as $\widetilde{n}(\varphi, 0)$ and $\widetilde{n}(\pi/2, \psi)$, respectively. They meet in the point $\widetilde{n}(\pi/2, 0) = (0, d + 1, 0)$.

At this point it is useful to re-parametrize also the weighted face image $f(u, v)$ given by Equ. (11):

$$\widetilde{f}(\varphi, \psi) = \begin{bmatrix} \widetilde{n}(\varphi, \psi) \\ r(\varphi)\widetilde{g}(\varphi) + s(\psi)\widetilde{h}(\psi) - a(d + 1) \end{bmatrix} \quad \text{where } a = g(\tfrac{\pi}{2}) = h(0).$$

In this representation, functions $\widetilde{g}(\varphi)$ and $\widetilde{h}(\psi)$ have a geometric meaning. Let us first look at $\psi = 0$. The planes $f(\varphi, 0)$ have the implicit equation

$$x_1 \cos \varphi + x_2 \sin \varphi + \widetilde{g}(\varphi) = 0. \tag{14}$$

Their envelope is a vertical cylinder whose intersection with the $x_1 x_2$ plane is a planar curve with support function $\widetilde{g}(\varphi)$, as can be clearly seen from Equ. (14). Analogously, the planes $f(\pi/2, \psi)$ have the implicit equation

$$x_2 \cos \psi + x_3 \sin \psi + \widetilde{h}(\psi) = 0. \tag{15}$$

Their envelope is a cylinder whose rulings are parallel to the x_1 axis and which intersects the $x_2 x_3$ plane in a curve whose support function is $\widetilde{h}(\psi)$.
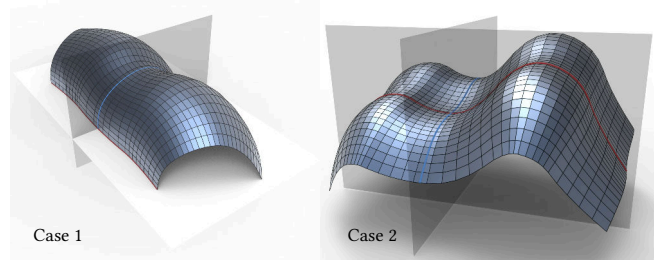
Fig. 17. Examples of conical PP meshes designed via their principal planar sections, using the explicit representations derived in §4.1.1 and §4.1.2.
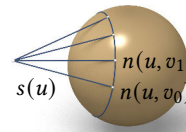
The two cylinders mentioned here are tangent to the surface $x(u, v)$ along parameter lines $x(u, 0)$ and $x(0, v)$ by construction. Thus they yield the apparent contour of the surface $x(u, v)$ when viewed in the x_3 direction and the x_1 direction. However, even more is true. Since the parameter lines of $x(u, v)$ are planar principal curvature lines, Prop. 2.2 implies that parameter lines $x(u, 0)$ and also $x(0, v)$ are orthogonal planar sections of the design surface $x(u, v)$.

We have thus reduced the design of the mesh (resp. the design of the surface $x(u, v)$) to the design of its principal planar sections. These can be chosen by the user. We recover the support functions $\widetilde{g}(\phi)$ and $\widetilde{h}(\psi)$, see Equ. (14), and enter them in the explicit representation of the weighted face image $\widetilde{f}(\phi, \psi)$. A conical PP mesh is recovered from $\widetilde{f}(\phi, \psi)$ by arbitrary sampling. Fig. 17 shows an example of this.

A similar computation can be performed in *Case 2*. Here $n(u, 0) = (u, 0, \frac{1}{2}(u^2 - 1))$ is a parabola with focal point in the origin. Its polar coordinate representation is $(r(\varphi) \cos \varphi, 0, r(\varphi) \sin \varphi)$, with $r(\varphi) = (\sin \varphi + 1)/\cos^2 \varphi$. Also $n(0, v)$ is a parabola with polar coordinate representation $(0, s(\psi) \cos \psi, s(\psi) \sin \psi)$, where $s(\psi) = (\sin \psi + 1)/\cos^2 \psi$. From here the computation of conical PP meshes is analogous to Case 1.

4.2 Conical P Meshes

4.2.1 Continuous Surfaces Analogous to Conical P Meshes.
For applications, already the P property may be useful, where only one of the 2 families of mesh parameter lines is planar. We therefore study conical P meshes in more detail. Their continuous counterparts are principal parametrizations $x(u, v)$ of surfaces with the additional property that each v parameter line is contained in a plane $W(u)$.

Recall Prop 2.2: The angle between the surface and $W(u)$ is constant along the parameter line, so it is a function $\alpha(u)$. It follows that the v parameter lines of the unit normal vector image $n(u, v)$ are circles. By the principal property, derivatives n_u, n_v are orthogonal, so the tangents of u parameter lines along a v parameter line form the rulings of a cone with a vertex $s(u)$. See inset figure.

4.2.2 Geometry of Conical P Meshes.
The case of conical P meshes is analogous to the continuous case described in the previous paragraph, but as it turns out, only approximately so. If all mesh parameter lines $\{v_{i,j}\}_{j \in \mathbb{Z}}$ are planar, the first paragraph of the proof

of Prop. 4.1 applies to the weighted normal image M_N°: The lines $\{n_{i+1,j}^\circ \vee n_{i,j}^\circ\}_{j \in \mathbb{Z}}$ spanned by transverse edges meet in the vertex S_i of a discrete cone. This situation is already shown in Fig. 15. The difference to the PP case is that now we cannot conclude that all S_i's lie on a straight line. Nor are parameter lines of M_N° circular.

For the applications we are interested in, meshes enjoy a certain amount of fairness, and their edges can be interpreted as derivatives. It is therefore reasonable to require that one family of mesh parameter lines of M_N° is circular.

4.2.3 Design of Conical P Meshes. Channel Surfaces. In theory we could design a conical P mesh M from a sequence of cone vertices S_i, which yields M_N°. M itself is found as a parallel mesh of $(M_N^\circ)^*$ according to Remark 4.1. This approach is not practical, however. We propose a different method of design in stages; from a guiding sequence of spheres to a channel surface to a general P surface. This method is based on the geometry of oriented spheres, so we will be able to use Laguerre geometry as introduced by § 2.1.

Step 1. The user chooses a sequence of (oriented) spheres by choosing their center and radius r. Using coordinates as in Equ. (1), this data is stored as vectors (x_j, y_j, z_j, r_j) and is considered as control polygon of a B-spline curve to create a continuous family of spheres $Z(t) = (z_1(t), \ldots, z_4(t))$. We use the tangential distance of Equ. (2) to uniformly sample $Z(t)$ and get a dense sequence of spheres $Z_1, Z_2, \ldots$

Step 2. We wish to find a watertight union of cones C_j that serves as a discrete envelope of the sphere sequence Z_j. We determine the cone C_j by its tangency to both Z_j and Z_{j+1} and clip it along the planes W_j, W_{j+1} containing the respective intersection with neighbours C_{j-1} and C_{j+1}. Practitioners of Laguerre geometry [Pottmann and Peternell 1998] know that the points contained in the plane W_j are exactly those spheres of radius 0 which obey

$$\langle\!\langle X - Z_j, H_j \rangle\!\rangle = 0, \ x_4 = 0, \ \text{where}$$
$$H_j = E_j + E_{j+1}, \quad E_j = \frac{1}{d(Z_j, Z_{j-1})}(Z_j - Z_{j-1}). \quad (16)$$

By comparing this formula with Euclidean geometry, we see that H_j is the normal vector of a bisector plane (in the sense of the Minkowski inner product) of edges $Z_{j-1}Z_j$ and Z_jZ_{j+1}. This computation is preferred over computing the intersection of algebraic surfaces C_j, C_{j+1}, because it is stable and it automatically yields the correct one of the two components of the complete intersection.

Step 3. We replace one cone, say C_{j_0}, by a sequence of tangent planes, clipped by planes W_{j_0-1} and W_{j_0}. This yields one row in a quad mesh enjoying two planar mesh parameter lines. We propagate this construction throughout the entire sequence of cones and get a quad mesh with the P property. It is even conical, since all faces incident with a vertex $v_{ij} \in W_j$ are tangent to the sphere Z_j. Some results can be seen in Fig. 18.

Step 4. Here we ask the designer for input again. We select a plane W_{j_0} and change the circular profile curve of the channel surface to an arbitrary profile curve. It is replaced by a profile polygon whose
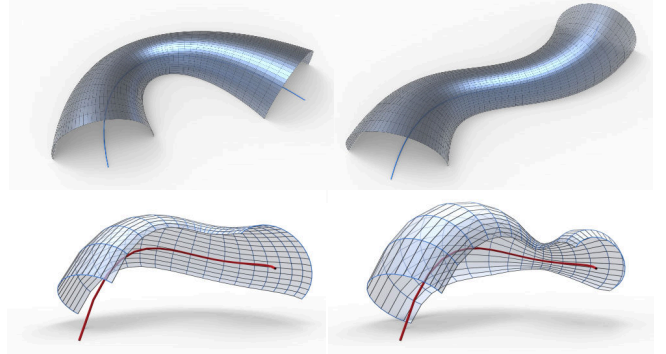

Fig. 18. Design of conical P meshes via the channel surface approach of § 4.2.3. Here we show Steps 2+3 of the construction. In the top row the radius function is the same for both examples shown, but the spine curve is different. In the bottom row the reverse is true.

edges are parallel to the edges of the channel surface's profile. We incrementally propagate this change to neighbours, maintaining the property that planes W_j carry mesh parameter lines. The conical property is not destroyed, because the new mesh is parallel to the original one. Figures 19 and 20 show examples created in this way. § 4.3 will discuss how further transformations are applied.

Remark 4.2 (Inflection points in profiles). The profile of Fig. 19, right, features inflection points. Such a profile can be edgewise parallel to a convex source profile only if the latter is traversed forwards for a time, and then backwards, and so on, changing direction every time an inflection point is reached.

Remark 4.3 (Semidiscrete surface representations). The semi-discrete surface representation in Step 2 is interesting in its own right for
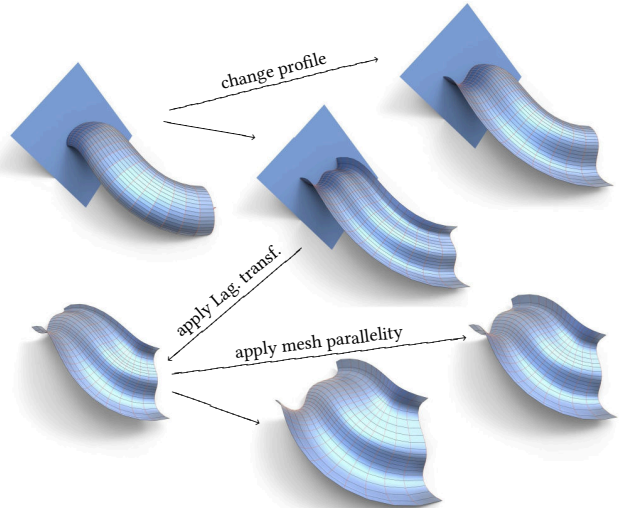

Fig. 19. Geometric design of conical P meshes via the channel surface approach of § 4.2.3. Step 4 of the construction consists of choosing a profile curve and propagating it along the spine curve. Afterwards Laguerre transforms and mesh parallelity are applied, see § 4.3.
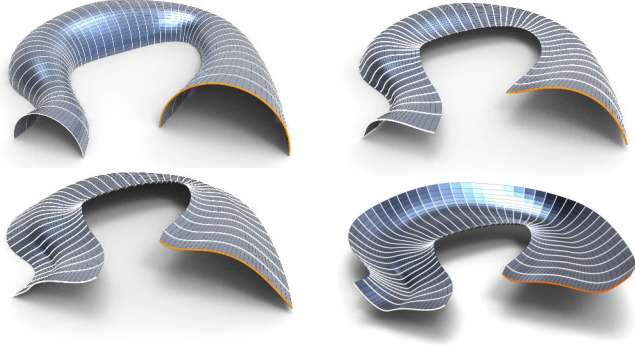
Fig. 20. Editing conical P meshes via changing profiles (Step 4 in the channel surface approach to design).
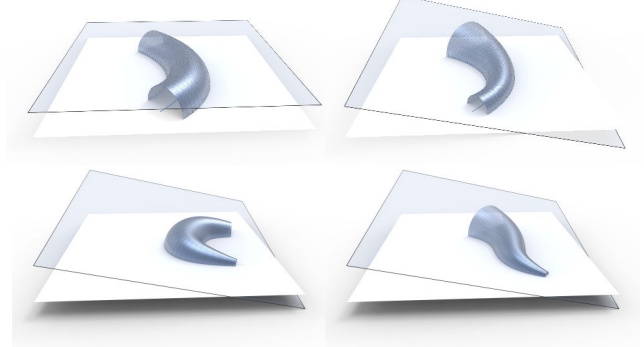

Fig. 21. Design of conical PP meshes via the channel surface approach of §§ 4.2.3 and 4.2.4. We demonstrate the results of Steps 2+3 with the additional ingredient of a common tangent plane T to ensure the PP property. The examples in the top row have the same spine curve but different plane T; for the bottom row the spine is changing, but the plane T is the same. In the language of § 4.1.1, this belongs to Case 1.
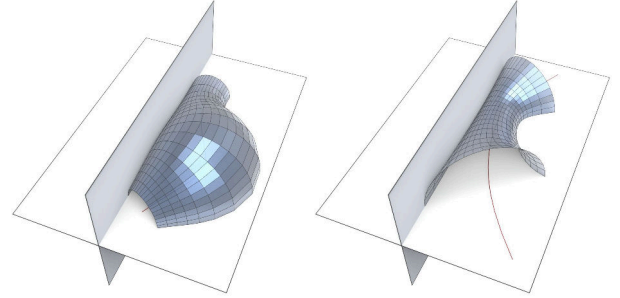

Fig. 22. Design of conical PP meshes via the channel surface approach of §§ 4.2.3, 4.2.4. Like in Fig. 21, we demonstrate the results of Steps 2+3 with an additional ingredient to ensure the PP property. We show the limit case where the two tangent planes exhibited by Fig. 21 have become one vertical plane, plus the requirement of symmetry w.r.t. the horizontal plane. In the language of § 4.1.1, this belongs to Case 2.

architecture applications. It can be extended to profiles in the form of arc splines, leading to surfaces consisting of cone patches.

Remark 4.4 (*Interpretation in terms of rotation-minimizing frames*). We constructed spheres Z_j as a uniform sample of a curve. If this uniformity is strictly true, Minkowski distances $d(Z_{j-1}, Z_j)$ are equal, and Equ. (16) shows there is a Minkowski reflection σ_j (in the bisector plane of edges $Z_{j-1}Z_j$ and Z_jZ_{j+1}) with obeys $\sigma_j(Z_{j-1}) = Z_{j+1}$. Obviously also cones are mapped by $\sigma_j(C_{j-1}) = C_j$. When discretizing cones in Step 3 by using their tangent planes, these too are related by σ_i. A further modification in Step 4 replaces meshes by parallel meshes (Figure 19) — we now have general discrete developables in between planes W_j, W_{j+1}. Still, the passage from one to the next is performed by σ_i. This reveals that the evolution of profiles as shown by Figure 19 is a discrete+Minkowski version of the motion of a *rotation-minimizing frame* along the discrete curve $\{Z_i\}$. For the RMF in general we refer to [Bergou et al. 2008], and for a treatment via reflections see [Wang et al. 2008].

4.2.4 Conical PP Meshes as Special Cases of Conical P Meshes.
The design procedure of § 4.2.3 is capable of creating conical PP meshes. If the spine curve lies in a plane M, and all spheres Z_i touch a plane T, then all spheres and cones involved are symmetric w.r.t. M, and the vertices of cones C_i lie in the line $M \cap T$. The intersection of an arbitrary pair of tangent planes of C_i meets $M \cap T$. For this reason the mesh constructed in Step 3 has edges which are either contained in the planes W_j, or edges lying in a plane through $M \cap T$. Thus, all mesh polylines are planar, and we have constructed a conical PP mesh. Examples are shown by Figure 21.

Another special case occurs if all spheres Z_i have the same radius r. Then the cones C_i are cylinders, and propagation of a mesh along the spine curve according to Step 3 is essentially done by the movement of a rotation-minimizing frame (see Remark 4.4). We mention a 3rd special case: If the spine curve lies in a horizontal base plane, planes W_j are vertical. This may be useful for architectural design.

4.3 Design of Conical P Meshes by Transformations
In § 4.2 we established the geometry of conical meshes which in addition enjoy the P property. We learned that neither mesh parallelism nor Laguerre transforms destroy these properties. Since the former do not change face normal vectors, and the latter cause

them to undergo a Möbius transform, we can simultaneously apply both kinds of transforms for geometric modeling, without having to implement general Laguerre transforms.

We use homogeneous coordinates $N = (n_1 : \ldots : n_4)$ for a normal vector $\frac{1}{n_4}(n_1, n_2, n_3)$. The condition of being a unit vector reads $n_1^2 + n_2^2 + n_3^2 = n_4^2$ and similar to Equ. (3) can be written as $N^T J N = 0$, where $J = \text{diag}(1, 1, 1, -1)$. § 2.1.2 states that a Möbius transform acts as $N \mapsto AN$, where the matrix A obeys $A^T J A = J$.

Consider now a conical P mesh (V, E, F). Each face f has a normal vector $N_f = (n_1 : \ldots : n_4)$ and is contained in a plane. The equation of that plane, using Cartesian coordinates $x = (x_1, x_2, x_3)$ is written as $\sum_{i=1}^3 n_i x_i + n_4 d_f = 0$. In block matrix notation this reads

$$\begin{bmatrix} x \\ d_f \end{bmatrix}^T \cdot N_f = 0.$$

When transforming the mesh, each vertex v contained in a certain face f gets mapped to a corresponding vertex $\bar{v}$ contained in the respective face $\bar{f}$ with normal vector $\bar{N}_f$ and scalar $\bar{d}_f$. Consequently,

$$\begin{bmatrix} \bar{v} \\ \bar{d}_f \end{bmatrix}^T \cdot AN_f = 0 \tag{17}$$
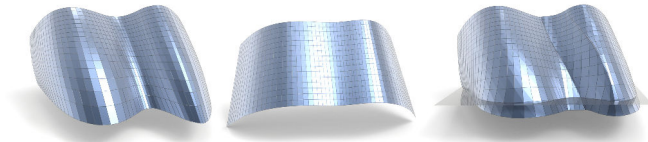
Fig. 23. Optimizing the PP mesh at left so that in addition it becomes conical, its shape changes dramatically (center). An effort to optimize such that even the previous shape is retained is unsuccessful: The result at right exhibits self-intersections, general lack of fairness, and non-planar faces.

holds whenever $v \in f$. These equations together with $A^T J A = J$ represent a system of quadratic constraints on the variables

$$A \in \mathbb{R}^{4 \times 4}, \quad \{\bar{d}_f\}_{f \in F}, \quad \{\bar{v}\}_{v \in V}.$$

The number of these variables is $4 \times 4 + |F| + 3|V|$. The user's input during interactive modeling can be incorporated as further constraints. Note that the full Laguerre transformation does not occur in this setup at all, only the Möbius transform as it operates on normal vectors.

The constraint system described here is quadratic and could be treated by the method of guided projection [Tang et al. 2014], using a combination of proximity to the previous state and fairness as regularizer. Our implementation is even simpler. When A is considered fixed, constraints become linear. So are user-imposed position constraints, and the entire system is solved in a least-squares sense, together with the aforementioned regularizers. In this way the parallel meshes of Fig. 19 have been created. We apply the same principle with A as a variable and disregarding the constraint $A^T J A = J$. A subsequent projection onto the set of admissible matrices can be performed via a Minkowski-polar decomposition [Higham 2003; Kintzel 2005]; see Figures 19 and 24 for examples.

5 CONCLUSION

In this paper we have shown many different approaches to the geometric design of meshes with planar faces equipped with various kinds of torsion-free support structures. In particular we treated planarity of mesh parameter lines (properties P and PP), and angle conditions which lead to principal meshes. The more conditions are imposed, the more special the methods of geometric design have to be. In some highly constrained cases (conical PP meshes) we employed an analogy to the continuous case to find explicit constructions of such meshes. In other cases (PP meshes) we showed to which extent design freedom exists, and we were able to suggest a spline-based design method. Only if comparatively few special properties are imposed, straightforward global optimization can be used. This is the case where meshes already have planar faces and we wish to additionally impose the P property.

Evaluation. In this paper we discuss the geometric design of highly constrained meshes, which is not easy with previous methods. Methods based on optimization in principle can be extended to include the P and PP properties, and indeed this works in some cases (see § 3.3). For more highly constrained meshes however, such as the conical meshes, simply adding the P and PP properties as optimization targets will likely not succeed, see Fig. 23 for an example

for making a PP mesh conical. Similarly, forcing a principal mesh to enjoy the PP property causes optimization to fail.

Even if optimization succeeds it is hardly an efficient way of design. This is not only because optimization is time-consuming. An additional reason is that a conical mesh with the P or PP property corresponds to a surface whose principal curvature lines are planar. The shapes of such meshes are therefore restricted, and achieving the P or PP property via optimization inevitably changes the shape of the mesh. It is hard to predict if optimization succeeds at all, and if it does, how much it will change the shape.

For this reason we do not expect that previous methods for constructing conical meshes can be extended to accommodate planar polylines. The same goes for torsion-free support structures, which like conical meshes are in relation to principal curvature lines [Pottmann et al. 2007]. In order to nevertheless enable design we developed the classification and construction results of §4.

Limitations. The different methods for design presented in this paper each have their limitations. Optimization for the P property (§ 3.3) will likely work only if planarity of faces is already established and mesh polylines can be interpreted as fair discrete curves – otherwise one cannot expect that straightforward optimization can achieve planar faces. This is because a mesh with planar faces is analogous to a network of conjugate curves on a surface, and so this property has implications on the mesh connectivity [Liu et al. 2006]. Other methods of design are based on *faces*, which can be called a dual approach to the problem (§ 3.2). Its limitations are mostly the difficulties inherent in handling dual elements, viz., planes. Finally, the highly constrained meshes discussed in § 4 experience a fundamental geometric limitation: They can no longer assume arbitrary shapes and have to be accessed by explicit constructions. While this is certainly a limitation from the mathematical viewpoint, it may not feel like one for applications in architecture, where one interactively explores the design space.

Summing up, we hope that this comprehensive discussion together with proposals for geometric design will be helpful for the actual realization of freeform architectural designs.

ACKNOWLEDGMENTS

REFERENCES

Sigrid Adriaenssens, Laurent Ney, Eric Bodarwe, and Chris J.K. Williams. 2012. Finding the form of an irregular meshed steel and glass shell based on construction constraints. *J. Architectural Engineering* 18 (2012), 206–213.

Rami Ballas. 2003. The Sail Tower, Haifa, Israel. *Structural Eng. International* 13, 3 (2003), 155–157.

Marcel Berger. 1987. *Geometry II.* Springer.

Miklós Bergou, Max Wardetzky, Stephen Robinson, Basile Audoly, and Eitan Grinspun. 2008. Discrete elastic rods. *ACM Trans. Graphics* 27, 3 (2008), 63:1–12.

Wilhelm Blaschke. 1929. *Vorlesungen über Differentialgeometrie.* Vol. 3. Springer.

Alexander Bobenko, Helmut Pottmann, and Thilo Rörig. 2020. Multi-nets: Classification of discrete and smooth surfaces with characteristic properties on arbitrary parameter rectangles. *Discrete and Computational Geometry* 63 (2020), 624–655.

Alexander I. Bobenko and Yuri B. Suris. 2007. On organizing principles of discrete differential geometry. Geometry of spheres. *Russian Math. Surveys* 62 (2007), 1–43.
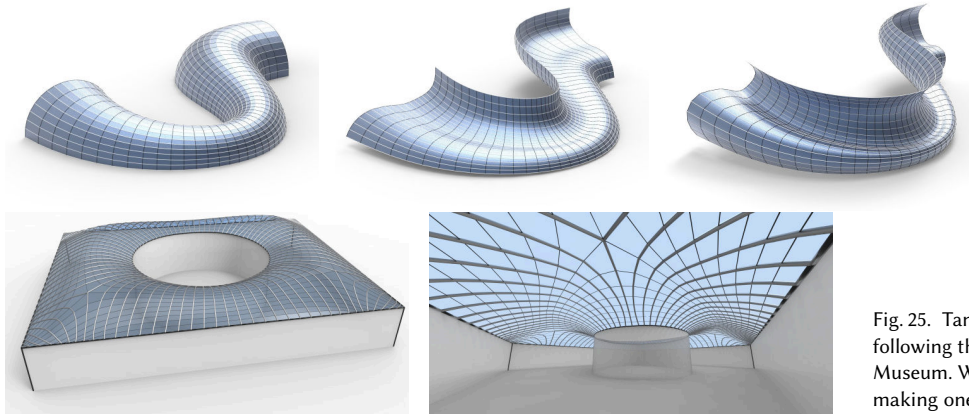
Fig. 24. Editing the conical P mesh at left by applying a profile change (center) and an additional Laguerre transformation (right).

Fig. 25. Tang et al. [2014] exhibit a mesh with planar faces following the shape of the Great Court roof of the British Museum. We additionally optimized it for the P property, making one half of mesh parameter lines planar.

Alexander I. Bobenko and Yuri B. Suris. 2008. *Discrete differential geometry. Integrable structure.* American Math. Soc.

Ossian Bonnet. 1853. Mémoire sur les surfaces dont les lignes de courbure sont planes ou sphériques. *J. Ecole Impériale Polytechnique* 20 (1853), 118–81.

Thomas Cecil. 1992. *Lie Sphere Geometry.* Springer.

Gaston Darboux. 1896. *Leçons sur la théorie générale des surfaces.* Gauthier-Villars.

Manfredo do Carmo. 1976. *Differential geometry of curves and surfaces.* Prentice-Hall.

Gershon Elber and Myung-Soo Kim. 1998. The bisector surface of rational space curves. *ACM Trans. Graphics* 17, 1 (1998), 32–49.

Yerab Ermias, Bar Shabtai, and Peter Szerzo. 2013. The courtyard roof of the museum of Hamburg History. In *Evolution of German Shells (2013 course and exhibition)*. Dept. Civil & Environ. Engrg., Princeton Univ. http://shells.princeton.edu/Ham.html

Nicholas Higham. 2003. J-orthogonal matrices: properties and generation. *SIAM Rev.* 45 (2003), 504–519.

Ulric Kintzel. 2005. Procrustes problems in finite dimensional indefinite scalar product spaces. *Lin. Algebra App.* 402 (2005), 1–28.

Hippolyte-Guillaume Lemonier. 1868. *Mémoire sur les surfaces dont les lignes de courbure sont planes ou sphériques.* Thunot, Paris.

Yang Liu, Helmut Pottmann, Johannes Wallner, Yong-Liang Yang, and Wenping Wang. 2006. Geometric modeling with conical meshes and developable surfaces. *ACM Trans. Graphics* 25, 3 (2006), 681–689.

Kaj Madsen, Hans Bruun Nielsen, and Ole Tingleff. 2004. *Methods for non-linear least squares problems* (2nd ed.). Technical Univ. Denmark.

James McCrae, Karan Singh, and Niloy J. Mitra. 2011. Slices: a shape-proxy based on planar sections. *ACM Trans. Graph.* 30, 6 (2011), 1–12.

Romain Mesnil, Cyril Douthe, Olivier Baverel, and Bruno Léger. 2017. Marionette Meshes: modelling free-form architecture with planar facets. *Int. J. Space Structures* 32 (2017), 184–198.

Romain Mesnil, Cyril Douthe, Olivier Baverel, and Bruno Léger. 2018. Morphogenesis of surfaces with planar lines of curvature and application to architectural design. *Automation in Construction* 95 (2018), 129–141.

Gaspard Monge. 1809. *Application de l'analyse a la géométrie.* Bernard, Paris.

Martin Peternell. 2000. Geometric properties of bisector surfaces. *Graphical Models* 62 (2000), 202–236.

Helmut Pottmann, Yang Liu, Johannes Wallner, Alexander Bobenko, and Wenping Wang. 2007. Geometry of multi-layer freeform structures for architecture. *ACM Trans. Graphics* 26, 3 (2007), 65:1–11.

Helmut Pottmann and Martin Peternell. 1998. Applications of Laguerre geometry in CAGD. *Comput. Aided Geom. Design* 15 (1998), 165–168.

Helmut Pottmann and Johannes Wallner. 1999. Approximation algorithms for developable surfaces. *Comput. Aided Geom. Design* 16 (1999), 539–556.

Volker Schmid, Jan-Peter Koppitz, and Anja Thurik. 2011. Neue Konzepte im Holzbau mit Furnierschichtholz – Die Holztragkonstruktion des Metropol Parasol in Sevilla. *Bautechnik* 88 (2011), 707–714.

Hans Schober. 2015. *Transparent shells: form, topology, structure.* Ernst & Sohn.

Yuliy Schwartzburg and Mark Pauly. 2013. Fabrication-aware design with intersecting planar pieces. *Comput. Graph. Forum* 32 (2013), 317–326.

Josep-Alfred Serret. 1853. Mémoire sur les surfaces dont toutes les lignes de courbure sont planes ou sphériques. *J. math. pures et appliqu.* 18 (1853), 113–162.

Werner Sobek and Lucio Blandini. 2010. The Mansueto library – notes on a glazed steel grid shell from design to construction. In *Challenging Glass 2.* 179–185.

Chengcheng Tang, Xiang Sun, Alexandra Gomes, Johannes Wallner, and Helmut Pottmann. 2014. Form-finding with polyhedral meshes made simple. *ACM Trans. Graph.* 33, 4 (2014), 70:1–9.

Xavier Tellier. 2020. *Morphogenesis of curved structural envelopes under fabrication constraints.* Ph. D. Dissertation. Univ. Paris-Est.

Xavier Tellier, Cyril Douthe, Laurent Hauswirth, and Olivier Baverel. 2019. Surfaces with planar curvature lines: discretization, generation and application to the rationalization of curved architectural envelopes. *Automation in Construction* 106, Article 102880 (2019).

Etienne Vouga, Mathias Höbinger, Johannes Wallner, and Helmut Pottmann. 2012. Design of self-supporting surfaces. *ACM Trans. Graphics* 31, 4 (2012), 87:1–11.

Wenping Wang, Bert Jüttler, Dayue Zheng, and Yang Liu. 2008. Computation of rotation minimizing frames. *ACM Trans. Graphics* 27 (2008), 2:1–18.

APPENDIX

Explicit Computation of Conical PP Surfaces and Their Geometric Design. The smooth surface $x(u, v)$ referred to in § 4.1.2 can be computed explicitly and has the following form: In case (1) we get

$$\begin{bmatrix} x_1 \\ x_2 \\ x_3 \\ x_4 \end{bmatrix} = \begin{bmatrix} d[(g+h)\sin u \cosh v + \dot{g}\cos u \cosh v - \dot{h}\sin u \sinh v] + \dot{g} \\ e[(g+h)\cos u \cosh v - \dot{g}\sin u \cosh v - \dot{h}\cos u \sinh v] \\ -(g+h)\cos u \sinh v + \dot{g}\sin u \sinh v + \dot{h}\cos u \cosh v + d\dot{h} \\ -e(\cos u + d\cosh v) \end{bmatrix}.$$

The most relevant information contained in this formula is the fact that $x(u, v)$ depends on functions g, h linearly. Case (2) is similar:

$$\frac{1}{x_4}\begin{bmatrix} x_1 \\ x_2 \\ x_3 \end{bmatrix} = \frac{1}{u^2 + v^2 + 1}\begin{bmatrix} (u^2 - v^2 - 1)\dot{g} + 2uv\dot{h} - 2u(g+h) \\ (v^2 - u^2 - 1)\dot{h} + 2uv\dot{g} - 2v(g+h) \\ 2(g+h-u\dot{g}-v\dot{h}) \end{bmatrix}.$$

The planes which carry parameter lines are given by the partial derivatives f_u, f_v, in direct analogy to the discrete case. In case (1), we have $f_u = (e\cos u, -d\sin u, 0, \dot{g})$, so the planes $V(u)$ are parallel to the x_3-axis and are tangent to a curve in the $x_1 x_2$ plane. A similar computation shows that the planes carrying the v parameter lines read $f_v = (0, \sinh v, e\cosh v, \dot{h})$. They are parallel to the x_1 axis, and are tangent to a certain envelope curve in the $x_2 x_3$ plane.

The significance of this remark is the following: If the geometric shapes of the aforementioned curves are given, functions $\dot{g}(u)$, $\dot{h}(v)$ can be reconstructed: Find the point parameter value u where $\begin{bmatrix} e\cos u \\ -d\sin u \end{bmatrix}$ is a normal vector and read off $\dot{g}(u)$ from the curve's tangent there; subsequently reconstruct g by integration. An analogous procedure works for h. We conclude that apart from offsets caused by the ambiguity in integration, the surface $x(u, v)$ is uniquely determined by the shape of two 2D curves.

It is not difficult to discuss simple cases. E.g. when both curves degenerate to points, $x(u, v)$ is a Dupin cyclide or a sphere.